JOURNAL OF AIRCRAFT
Vol. 43, No. 5, September–October 2006

Stability and Control Characteristics of a New FAR 23 Airplane

Kasim Biber*
Biber Aeronautical Research, 34870 Istanbul, Turkey

Wind-tunnel tests were conducted for a power-off and stick-fixed 1/12 scale model of a high-wing FAR 23 cargo transport airplane at Reynolds number 0.92×10^6 and Mach number 0.2. Tests included simultaneous measurements of six-component force and moment using the tunnel external balance. Effects of flap, elevator, rudder, and aileron on longitudinal and lateral-directional aerodynamics were investigated in a stability-axis system. Pertinent static stability and control derivatives were obtained and used for the analysis of airplane open-loop dynamic stability and response. The airplane in its cruise flight phase appears to achieve better than level 3 longitudinal flying qualities. Changes are suggested in size and shape of airplane components for improvement in design.

Nomenclature

C_D, C_L, C_Y	=	drag, lift, and side force coefficient
C_{D0}	=	drag coefficient for zero angle of attack
C_{D1}	=	drag coefficient for flight
C_{L0}	=	lift coefficient for zero angle of attack
C_{L1}	=	lift coefficient for flight
$C_{L\max}$	=	maximum lift coefficient
C_M, C_n, C_l	=	pitching, yawing, and rolling moment coefficients
C_{MCL}	=	variation of pitching moment coefficient with lift coefficient
$C_{L\alpha} C_{D\alpha}, C_{M\alpha}$	=	lift, drag, and pitching moment coefficient slopes
$C_{L\dot{\alpha}}, C_{M\dot{\alpha}}$	=	variation of lift and pitching moment coefficients with rate of change of angle of attack
$C_{L\delta f}$	=	variation of lift coefficient with flap angle
$C_{L\delta e}, C_{D\delta e}, C_{M\delta e}$	=	variation of lift, drag, and pitching moment coefficients with elevator angle
C_{Lu}, C_{Du}, C_{Mu}	=	variation of lift, drag, and pitching moment coefficients with air speed
$C_{l\beta}, C_{n\beta}, C_{Y\beta}$	=	variation of rolling, yawing, and side force coefficients with sideslip angle
$C_{l\delta r}, C_{n\delta r}, C_{Y\delta r}$	=	variation of rolling, yawing, and side force coefficients with rudder angle
$C_{l\delta a}, C_{n\delta a}, C_{Y\delta a}$	=	variation of rolling, yawing, and side force coefficients with aileron angle
C_{lp}, C_{np}, C_{Yp}	=	variation of rolling, yawing, and side force coefficients with roll rate
C_{lq}, C_{nq}, C_{Yq}	=	variation of rolling, yawing, and side force coefficients with pitch rate
C_{lr}, C_{nr}, C_{Yr}	=	variation of rolling, yawing, and side force coefficients with yaw rate
c	=	mean aerodynamic chord
I_{xx}, I_{yy}, I_{zz}	=	rolling, pitching, and yawing moments of inertia
i_h, i_w	=	horizontal stabilizer and wing incidence angle
L/D	=	lift-to-drag ratio
N_0	=	neutral point
P	=	period
p, q, r	=	roll, pitch and yaw rate
S	=	wing area
$T_{1/2}, N_{1/2}$	=	time and cycle to damp-to-half amplitude
W	=	airplane maximum weight
X, Y, Z	=	wind tunnel coordinate axes
α	=	angle of attack
β	=	sideslip angle
$\Delta q, \Delta q, \Delta r$	=	change in roll, pitch, and yaw rate
Δu	=	change in horizontal velocity
$\Delta\alpha$	=	change in angle of attack
$\Delta\delta$	=	change in control deflection
$\Delta\theta, \Delta\beta, \Delta\phi$	=	change in pitch, sideslip, and bank angle
δ_{al}, δ_{ar}	=	left and right aileron angle
$\delta_f, \delta_e, \delta_r, \delta_a$	=	flap, elevator, rudder and aileron deflection angle
ε	=	downwash angle
ζ	=	damping ratio
λ	=	eigenvalue
τ	=	roll time constant
ψ	=	yaw angle
ω_n	=	undamped natural frequency

Received 30 August 2005; revision received 14 October 2005; accepted for publication 14 October 2005; presented as Paper 2006-0255 at the 44th Aerospace Sciences Meeting and Exhibit, Reno, NV, 9–12 January 2006.

*Research Engineer, Karliktepe Mah, Serap Sok, No 4/10, Kartal; kxbiber@yahoo.com. Senior Member AIAA.

Introduction

THERE has been growing interest in design and development of a new cost-effective and relatively short-range cargo transport airplane. This airplane should carry 4 LD-3 or 4 DEMI or mixed standard containers having 3402-kg (7500-lb) revenue payload over 250 n mile. For centerline thrust and reliability, it should also be equipped with a twin-pack engine driving a single propeller through a unique combining gearbox.

Figure 1 shows the airplane three-view having a high wing, conventional tail, fixed nose, and main landing gear. Maximum takeoff weight is 8618 kg (19,000 lb), considered as the certification limit for the FAR-23 commuter category.[1] Flight performance has been reported in companion publications.[2–4] Because of its unique design features, two-phase wind-tunnel tests were conducted on a power-off and stick-fixed 1/12 scale model of this airplane. The tests included the investigation of flap, elevator, rudder, and aileron deflection on longitudinal and lateral-directional aerodynamics.

The purpose of this paper is to report the first phase of these wind-tunnel tests and to provide static stability and control derivatives. The derivative data were used to determine the open-loop dynamic stability and response characteristics, followed by an analysis to evaluate the airplane's flying qualities. Based on the analysis, suggestions are made for changes in size and shape of the airplane components for improvements in design. The suggested changes were incorporated into the airplane configuration shown in Fig. 1. The data presentation is made only for the flaps-up configuration, considered as a baseline.

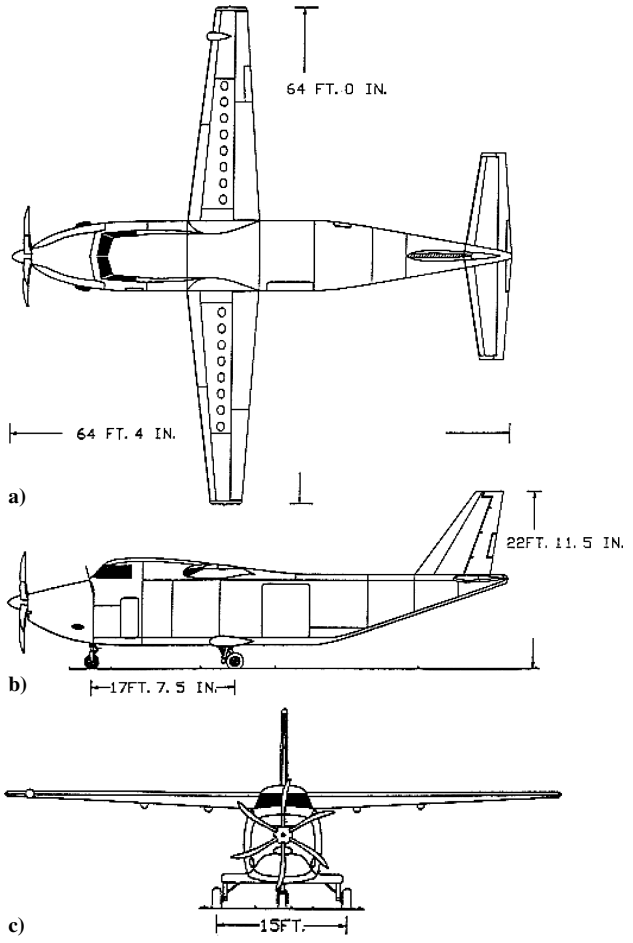

Fig. 1 Airplane three-view geometry: a) top, b) side, and c) front view.

Experimental Procedure

Wind Tunnel

The experiments were conducted in the Wichita State University low-speed wind tunnel,[5] which has a 2.13-m (7-ft)-high, 3.05-m (10-ft)-wide, and 3.66-m (12-ft)-long test section. It is a closed-return tunnel with atmospheric test-section pressure. The tunnel is equipped with a pyramidal external balance and Hewlett Packard 380 computer system for six-component force and moment data acquisition and reduction. The raw data are acquired from six balance channels as averages of 1024 samples of voltage readings and then converted to forces and moments. Tunnel wall corrections are applied to the force and moment data. These corrections are buoyancy drag, solid and wake blockage, and streamline curvature in three dimensions as described in Ref. 6. The data reduction is made in a wind-axis system in which the test section centerline is considered as the horizontal. The test data can then be converted to the body and stability-axis system, as desired. The tunnel coordinate axes consisted of X, Y, and Z components and had their origin at the model center of gravity. The center of gravity was located at the quarter-wing mean aerodynamic chord. The X-axis was in the plane of airplane symmetry and positive in the upstream direction. The Z-axis was also in the plane of symmetry and positive downward. The Y-axis, on the other hand, was perpendicular to the plane of symmetry and positive along the right wing. The resolution in the tunnel instrumentation is as follows: for lift, ± 0.9 N and ± 0.001 (ΔC_L); for drag, ± 0.2 N and ± 0.0003 (ΔC_D); for pitching moment, ± 0.1 N-m and ± 0.0003(ΔC_M); for dynamic pressure ± 4.8 N/m^2; for pressure transducers ± 2.4 N/m^2 and ± 0.002 (ΔC_P); and for angle of attack ± 0.05 deg.

Test Model

The test model was 1/12 the scale of the cargo transport airplane. It had a 1.83-m (6-ft) span in a 3.05-m (10-ft)-wide test section. The fuselage and lifting surfaces were built all separate and then assembled together for the complete model. The wing was made of solid aluminum in three pieces. For the present tests, it had a NACA 4412 airfoil with constant chord. The modified configuration (Fig. 1) was, however, equipped with a custom design having maximum thickness 18%c root and 13%c tip airfoil. Flap, aileron, elevator, and rudder were positioned using different brackets for their angular setting. Tail surfaces were of conventional design and made of solid aluminum with a NACA 0012 airfoil section. They were removed for tail-off wing–fuselage tests. The airplane is projected to have fixed landing gear, and therefore, the tricycle gear arrangement were, maintained throughout the test program. The main and nose landing gear were, however, removed from the fuselage in the last portion of tests to investigate gear effects. The model was installed in the test section using a three-point mount system.

Test Conditions

All tests were made at a dynamic pressure of 268.5 kg/m^2 (55 lb/ft^2), imposed by the tunnel conditions and model strength. This corresponds to a chord-based Reynolds number of 0.92×10^6 and Mach number of 0.2. To improve the Reynolds number effects, the boundary layer transition was fixed by two layers of 2.54-mm (0.1-in.)-wide and 0.02-mm (0.0008-in.)-thick strips at 5% fuselage length, wing chord, and horizontal and vertical stabilizer locations. Tufts and oil flow were used on the model surface to visualize the boundary-layer flow patterns.

Test Matrix

The complete test program was performed in a series of 108 tunnel runs. These runs were scheduled in such a way that the minimum amount of time was spent for the model change. The pitch sweep was made at yaw angles $\psi = 0$, 4, and 8 deg with angle of attack α ranging from -8 to 22 deg. The yaw sweep was made at $\alpha = 0$ and 6 deg with ψ ranging from -4 to $+16$ deg. Wing flaps had deflections of 10, 20, and 30 deg. The elevator, rudder, and aileron powers were determined for both flaps up and down 30-deg cases. However, this paper presents the test data for only the flaps-up baseline configuration. The derivatives in general represent the slopes of the best-fit linear data line from the origin of the axis system. For pitch runs, they were obtained for the range of angles of attack that corresponds to the linear lift curve.

Results and Discussion

Longitudinal Aerodynamics

Longitudinal aerodynamics was investigated from pitch runs conducted at zero yaw. Figure 2 shows C_L–α curves for flap angles of 0, 10, 20, and 30 deg. Tail-off cases are also included for comparison. The lift coefficient at $\alpha = 0$ deg is 0.298 when $\delta_f = 0$ deg, and it becomes 0.925 when $\delta_f = 30$ deg. From this C_L–δ_f relation, the flap effectiveness, $C_{L\delta f}$, is obtained as 1.215/rad. The maximum lift coefficient is 1.398 for the flaps-up case having stall angle 15.6 deg, and it becomes 1.775 for the flaps-down 30-deg case with stall angle 11.65 deg. The flaps are apparently not effective in

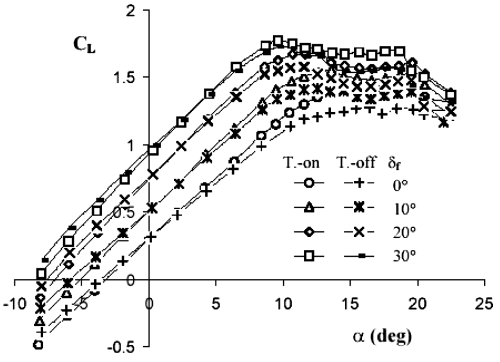

Fig. 2 Lift characteristics for flap angles of 0, 10, 20, and 30 deg, including tail-off cases.

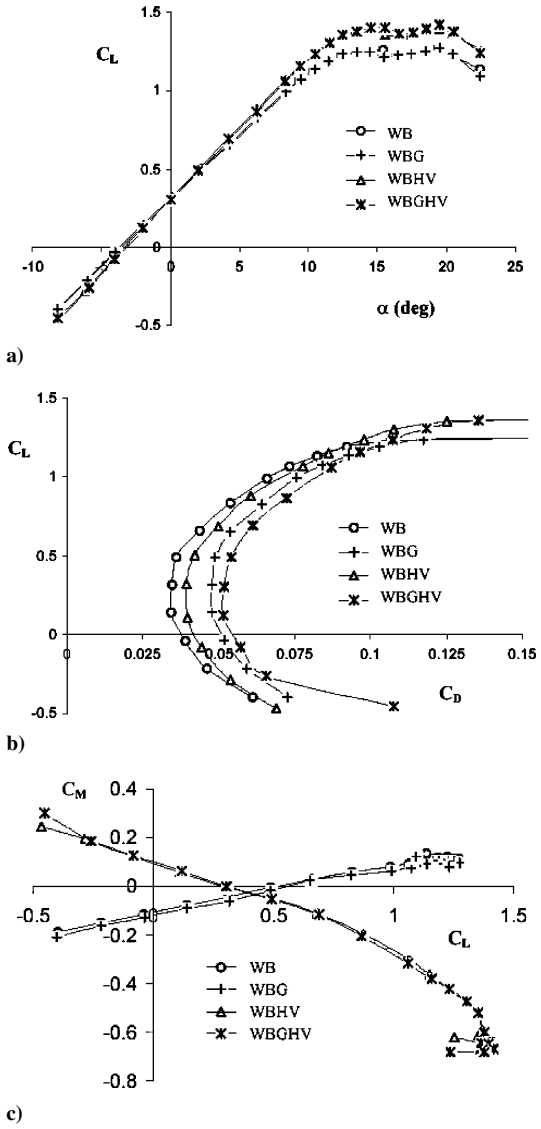

Fig. 3 Effect of gear and horizontal and vertical tail components on a) lift coefficient, b) drag coefficient, and c) pitching moment coefficients.

Table 1 Configuration build up for C_L and C_D data

Conf	α_0, deg	$C_{L\alpha}$, 1/rad	C_{L0}	$C_{L\max}$	C_{D0}
WB	−3.61	4.778	0.297	1.262	0.0344
WBG	−3.58	4.784	0.296	1.248	0.0477
WBHV	−3.23	5.283	0.293	1.393	0.0393
WBGHV	−3.24	5.283	0.297	1.402	0.0518

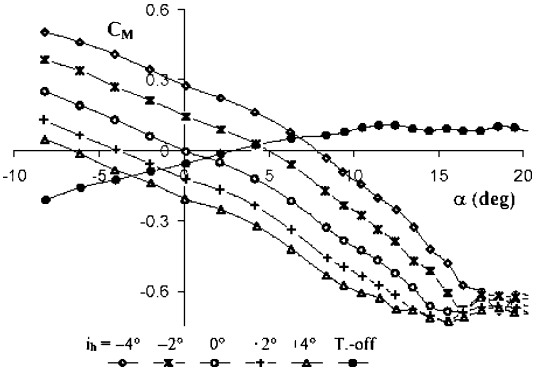

Fig. 4 C_M variation with α at horizontal setting from −4 to +4 deg, including tail-off.

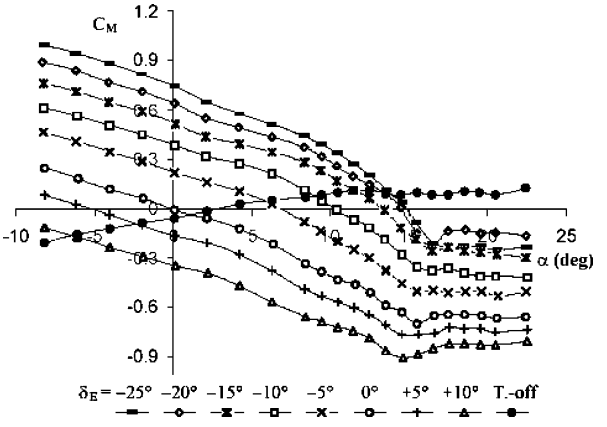

Fig. 5 C_M variation with α at elevator angles from −25 to +10 deg, including tail-off.

producing the amount of lift increment needed for high performance. Removing tail surfaces results in a decrease of lift-curve slope and $C_{L\max}$. The $C_{L\max}$ contribution from the horizontal surface is 0.152 (10.8% of $C_{L\max}$) when $\delta_f = 0$ deg and 0.106 (5.8% of $C_{L\max}$) when $\delta_f = 30$ deg.

Figure 3 shows the effect of gear and horizontal and vertical stabilizer components on lift, drag, and pitching moment coefficients. Table 1 provides the pertinent C_L and C_D characteristics taken from the figure. (W, wing; B, body; G, gear; H, horizontal; V, vertical.) Wing alone was not tested, but its $C_{L\alpha}$ was estimated to be 5.10/rad, about 10% lower than that of the complete model, as expected. Horizontal stabilizer addition has the effect of increasing $C_{L\alpha}$, $C_{L\max}$, and C_{D0}. It changes the C_M slope from positive to negative for static stability, as expected. The C_M curves have a difference in slope, C_{MCL}, of as much as −0.59, indicating the stability contribution from the horizontal surface. The model is trimmed when $C_L = 0.311$. Gear addition causes a substantial increase, as much as 25%, in C_{D0}. For the complete model, the span efficiency factor, e, was estimated to be 0.81 from a plot of C_L^2 with C_D for the tail-off case, as described in Ref. 7. Maximum lift-to-drag ratio, L/D, is 12.18.

The incidence for the horizontal stabilizer, i_h, was varied over a range to determine its optimum setting and the corresponding downwash angle. Figure 4 shows the C_M variation with α for incidences from −4 to +4 deg, including the tail-off. The equilibrium ($C_M = 0$) is obtained when $i_h = 0$ deg, and therefore, zero incidence was used for the rest of the horizontal setting. This was for the convenience of tests. The horizontal tail incidence is normally set such that $C_M > 0$ at $\alpha = 0$ deg for positive static stability. Downwash angle can be determined from the C_M curves. As described in Ref. 6, the intersections of tail-on curve with tail-off curve are points where, for a given wing angle of attack, α_w, tail-on and off C_M values are equal; that is, the tail is at zero lift. Therefore, the horizontal angle of attack $\alpha_h = \alpha_w + i_h - \varepsilon = 0$. Because α_h and i_h are known from the intersection points, ε may be determined and plotted against α_w. From this plot, the downwash derivative becomes $d\varepsilon/d\alpha = 0.27$. The downwash can have a significant effect on the tail for a high-wing configuration having a large propeller disk diameter. This was evident from the behavior of tufts and oil flow attached on wing and fuselage surfaces. Vortices developed on wing and fuselage juncture shed downstream and joined with those on the upper corners of fuselage constant section. They apparently reduced the effectiveness of tail and control elements.

Longitudinal stability was investigated from C_M curves obtained for various elevator angles. Figure 5 shows the C_M variation with α for elevator angles from −25 to +10 deg in 5-deg increments, including the tail-off. The elevator-up, that is, negative deflection has the effect of increasing airplane C_L. The elevator-down, that is, positive deflection, on the other hand, has the effect of decreasing C_L. The variation is almost linear up to the stall α. The slope of pitching moment coefficient, $C_{M\alpha}$, is −1.66/rad, indicating a stabile

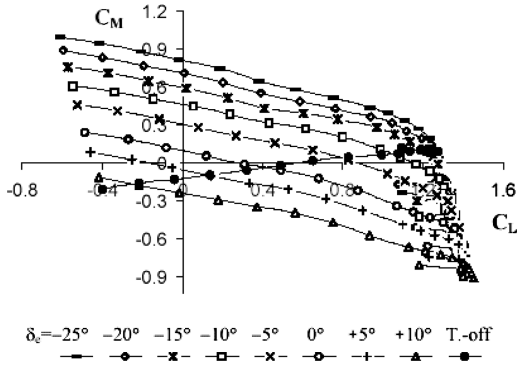

Fig. 6 C_M **variation with** C_L **at elevator angles from −25 to +10 deg, including tail-off.**

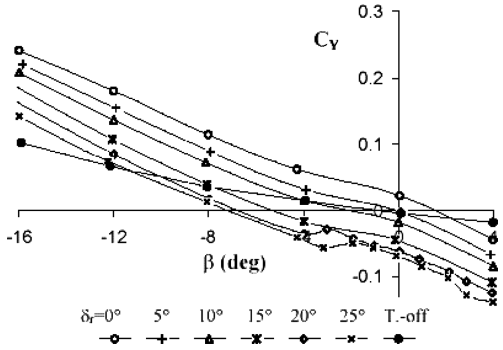

Fig. 7 C_Y **variation with** β **at rudder angles from 0 to 25 deg, including tail-off.**

airplane with flaps up. The C_M values at $\alpha = 0$ deg were used to determine the elevator power, which $C_{M\delta e} = -1.83$/rad. The elevator effectiveness is reduced for deflections beyond −25 deg.

Neutral point was determined by using the C_M variation with C_L as shown in Fig. 6. The slope of the C_M curve $C_{MCL} = -0.32$. For the baseline center of gravity at $0.25c$, the neutral point is located at $0.57c$. The slope becomes $-0.37c$ for $0.20c$ and $-0.17c$ for $0.40c$ center of gravity locations. Power effect, that is, the running propeller, would have a destabilizing effect on the longitudinal stability. This effect reduces the static margin of airplane by as much as $0.11c$, as estimated by the method of Ref. 7. The power effect is, however, not included with the data presentation.

Lateral-Directional Aerodynamics

Yaw runs were conducted at $\alpha = 0$ deg to study the effect of rudder deflection on side force and yawing and rolling moment. Figure 7 shows the variation of side force coefficient C_Y with sideslip angle β, including the tail-off case. The rudder was deflected to the right at $\delta_r = 0, -5, -10, -15, -20$, and -25 deg. It was assumed that the left rudder deflections would give the same results as the right deflections, due to the model symmetry. The model has positive side force with negative sideslip, as expected. At $\beta = -16$ deg, C_Y has a magnitude of 0.25 for tail-on and 0.1 for tail-off configuration. The difference shows the significance of the vertical stabilizer. The side-force coefficient due to sideslip has a derivative $C_{Y_\beta} = -0.86$/rad. Side force variation with rudder angle was determined and had a derivative, $C_{Y\delta r} = 0.23$/rad at zero-sideslip condition.

Figure 8 shows the variation of yawing moment coefficient, C_n, with β, including the tail-off case. The intersection of zero rudder with tail off is offset from the origin, indicating some model asymmetry. The airplane is, however, directionally stable with positive slope $C_{n\beta} = 0.132$/rad for all rudder deflections. The change of C_n with rudder deflections produces a slope $C_{n\delta r}$ of around 0.132/rad, which is the rudder power. The ratio of these two derivatives gives $d\beta/d\delta_r = 1$, the equilibrium value, meaning 1-deg sideslip for 1-deg rudder deflection. Roll stability is presented in Fig. 9, including the tail-off case. The slope $C_{l\beta}$ has a negative value of -0.115/rad,

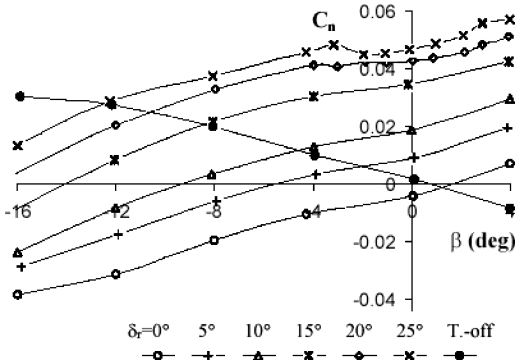

Fig. 8 C_n **variation with** β **at rudder angles from 0 to 25 deg, including tail-off.**

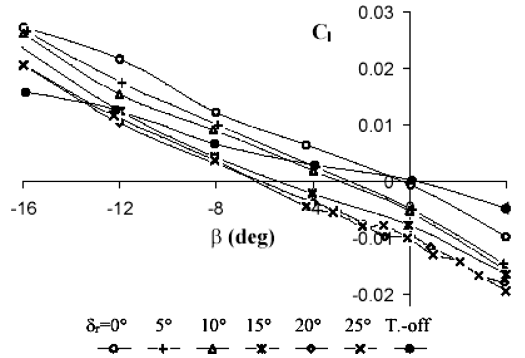

Fig. 9 C_l **variation with** β **at rudder angles from 0 to 25 deg, including tail-off.**

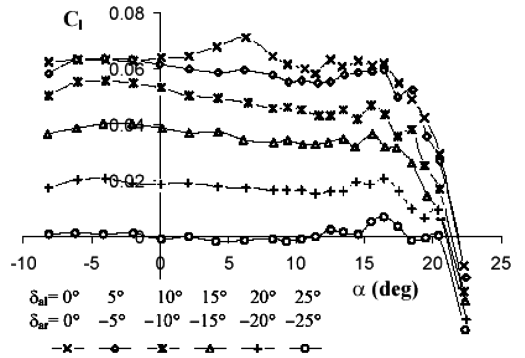

Fig. 10 C_l **variation with** α **at left and right aileron angles from 0 to ±25 deg.**

indicating an effective dihedral. Rolling moment coefficient C_l due to the rudder angle, $C_{\delta r}$, was determined to be 0.026/rad.

Pitch runs were conducted at zero yaw to investigate the effect of ailerons on rolling and yawing moment. The left aileron had positive-down deflections of 0, 5, 10, 15, 20, and 25 deg and the right aileron had negative-up deflections of 0, −5, −10, −15, −20, and −25 deg. This setup is meant to have a right roll due to adverse yaw produced in the right direction. The aileron tests were made with tail off because the downwash produced by the aileron is carried away in flight due to helix angle, but it is brought onto the horizontal tail as extra load in the wind tunnel.[6]

Figure 10 shows the aileron effects on rolling moment coefficient, C_l. Increase of aileron angle, δ_a, increases C_l until $\delta_a = 20$ deg. The maximum C_l is about 0.064, considered satisfactory for the test configuration. The C_l variation with α is almost constant until the stall condition. The aileron power $C_{l\delta a}$, is equal to 0.23/rad. The aileron loses its power gradually as its deflection increases to high angles. Figure 11 shows the aileron effects on C_n variation with α. Increase of aileron angle increases the slope $C_{n\alpha}$. The control derivative $C_{n\delta a}$ is −0.0115/rad.

Table 2 Static stability and control data[a]

Wind-tunnel data		Estimated data	
C_{L0}	0.303	$C_{L\dot{\alpha}}$	2.61
C_{D0}	0.0518	C_{Lq}	9.665
C_{M0}	0	C_{Lu}	0.027
$C_{L\alpha}$	5.357	$C_{D\alpha}$	0.191
$C_{L\delta e}$	0.286	C_{Txu}	−0.158
$C_{M\alpha}$	−1.662	$C_{M\dot{\alpha}}$	−14.614
$C_{M\delta e}$	−1.833	C_{Mu}	0
$C_{Y\beta}$	−0.859	C_{Mq}	−54.126
$C_{Y\delta r}$	0.229	C_{Yp}	0
$C_{Y\delta a}$	0	C_{Yr}	0.937
$C_{n\beta}$	0.132	C_{np}	−0.038
$C_{n\delta r}$	0.132	C_{nr}	−0.214
$C_{n\delta a}$	−0.011	C_{lp}	−0.893
$C_{l\beta}$	−0.108	C_{lr}	0.127
$C_{l\delta r}$	−0.0229		
$C_{l\delta a}$	0.212		

[a]Derivatives are given in 1/rad.

Table 3 Airplane data for cruise flight

Variable	Value
Altitude h, ft	10,000
Mach number, M	0.25
True airspeed U_1, ft/s	280
Center of gravity location, fraction c	0.25
Angle of attack α_1, deg	0
Weight W, lbs	19,000
I_{xx}, slug-ft^2	50,000
I_{yy}, slug-ft^2	45,000
I_{zz}, slug-ft^2	90,000
I_{xz}, slug-ft^2	0
C_{L1}	0.4
C_{D1}	0.0525
C_{TX1}	0.0525

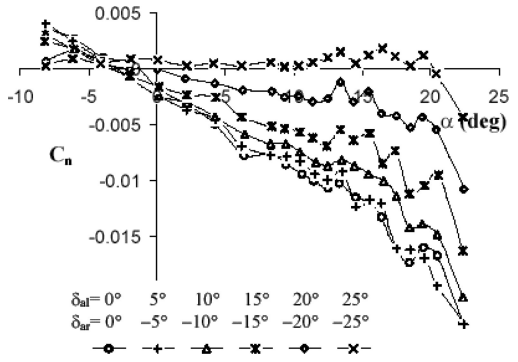

Fig. 11 C_n variation with α at left and right aileron angles from 0 to ±25 deg.

Longitudinal Motion and Response

The static stability and control data obtained from the wind tunnel were used to determine the airplane open loop dynamic stability and response characteristics. Table 2 has a summary of the data in addition to those calculated from the empirical methods.[8–11] The analysis was made for only cruise flight at 165 n mile, with the baseline center of gravity location at 0.25c. Table 3 contains airplane mass properties obtained from published data for similar airplanes.[12] The C_{L1} value corresponds to cruise level flight, and C_{D1} is obtained from the drag polar.

The airplane equation of motion is formulated in state space as $x' = Ax + \eta B$, where $x = [\Delta u, \Delta\alpha, \Delta q, \Delta\theta]^T$ is the state vector, $\eta = [\Delta\delta]$ is the control vector, and the matrices A and B contain dimensional stability and control derivatives, calculated using the corresponding values in Table 2. The matrix A, as defined in Ref. 10, has the following values for the longitudinal dynamics of the airplane:

$$A_{\text{long}} = \begin{bmatrix} -0.031 & 0.062 & 0 & -32.2 \\ -0.246 & -1.61 & 278.7 & 0 \\ 0.00142 & -0.039 & -7.545 & 0 \\ 0 & 0 & 1 & 0 \end{bmatrix}$$

Expanding this matrix yields a fourth-order characteristic equation of the form

$$A1\lambda^4 + B1\lambda^3 + C1\lambda^2 + D1\lambda + E1 = 0$$

The coefficients of the characteristic equation are $A1 = 281.6$, $B1 = 2565$, $C1 = 6421$, $D1 = 333.2$, $E1 = 107.4$. The eigenvalues for this characteristic equation describe the modes of motion:

1) short-period mode, $\lambda_{\text{long1,2}} = -4.578 \pm 1.472i$

2) phugoid mode, $\lambda_{\text{long2,3}} = -0.015 \pm 0.128i$

The eigenvalues are complex and have negative real parts. This means the airplane is dynamically stable. If the airplane were given an initial disturbance, the disturbance would decay in time sinusoidally.

The eigenvalues are expressed in terms of damping and frequency values, $\lambda_{1,2} = \eta \pm i\omega$, where $\eta = -\zeta\omega_n$ and $\omega = \omega_n(1-\zeta^2)^{1/2}$. The damping ratio, ζ, and undamped natural frequency, ω_n, along with the time to half amplitude, $T_{1/2}$, the period, P, and the number of cycles of half amplitude, $N_{1/2}$, are calculated for the short-period and phugoid motions. Table 4 contains the calculated values for the baseline configuration. Of these two modes, the short-period mode is of more importance because of its relatively high frequency and heavy damping, for which the airplane has a rapid respond to elevator input without any undesirable overshoot. If this mode had light damping and low frequency values, then the airplane would be difficult to control and possibly dangerous to fly. The phugoid or long-period mode has so small a frequency and such light damping that the pilot can easily negate disturbances by small control movements. It would, however, cause fatigue for the pilot if the damping were too low.

The damping and frequency of both the short- and long-period modes are in fact functions of aerodynamic stability derivatives. They can be controlled by changes in airplane geometric and aerodynamic characteristics. For example, increasing the tail size would increase both the static stability and damping of the short-period motion. However, the increased tail area would also increase the weight and drag of the airplane. This in turn would reduce the airplane's performance. There need to be an optimum performance that is both safe and easy to fly, and the stability and control required for the pilot to consider the airplane safe and flyable. This type of requirement for airplanes is regulated in flying qualities standards such as those given in MIL-F-8785C and MIL-HDBK-1797, Refs. 13 and 14. These documents contain a number of criteria to which the dynamic modes of an airplane can be compared to predict the expected flying-quality levels.

There are four levels of flying qualities. Level 1 implies that flying qualities of an aircraft are clearly satisfactory to perform a specific task with acceptable pilot workload at all times. At level 2, the aircraft still has adequate flying qualities, but the pilot workload has increased, or achievable task performance is reduced. Level 3 refers to the degradation of flying qualities such that the aircraft is controllable, but the task performance is inadequate, and the pilot workload is very high. Level 4 corresponds to situations where there is a high risk of loss of control. These levels of flying qualities are

Table 4 Longitudinal dynamic characteristics

Variable	Short-period	Phugoid
$T_{1/2}$, s	0.151	45.184
P, s	4.267	49.022
$N_{1/2}$, cycles	0.035	0.922
ζ	0.952	0.118
ω_n, cycles/s	0.765	0.129

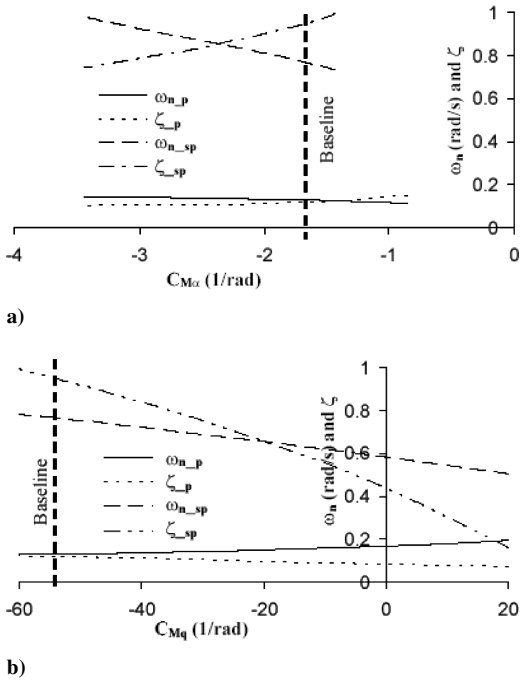

Fig. 12 Sensitivity analysis for ω_n and ζ parameters with changes in stability derivatives: a) $C_M\alpha$ and b) C_{Mq}.

defined with reference to the Cooper–Harper rating scale.[15] Cooper–Harper ratings of 1, 2, and 3 fall in level 1, whereas 4, 5, and 6 are in level 2, and 7, 8, and 9 are in Level 4. References 9, 10, and 11 have these ratings expressed graphically for short-period motion as a function of ω_n and ζ values. Based on those graphical displays, the present cargo-transport airplane for its cruise flight phase appears to achieve better than level 3 flying qualities. With regard to the phugoid mode, the airplane $\zeta = 0.118$, greater than 0, qualifying for level 2 flying qualities. The airplane configuration apparently needs some changes to improve its longitudinal flying qualities.

The sensitivity of short-period ω_n and ζ values to changes in stability derivatives was investigated. The longitudinal stability derivative, $C_{M\alpha}$, is of importance, because of its dependence on the location of center of gravity. Figure 12 shows the effect of the $C_{M\alpha}$ variation on dynamic stability characteristics. The baseline values correspond to the $C_{M\alpha}$ value of the present configuration. Increase of $C_{M\alpha}$ (less negative) means moving the X center of gravity aft toward its neutral point. As a result, ω_n decreases and ζ increases linearly for both the short-period and phugoid modes. Figure 12 shows the effect of another important stability derivative, C_{Mq}, on ω_n and ζ parameters. As C_{Mq} increases (becomes less negative) from the baseline value, the short-period ζ decreases significantly. This shows the powerful effect of C_{Mq} on the damping ratio of the short-period mode.

An analysis was made to determine the free longitudinal response of the airplane for a given initial disturbance. For this reason, the fourth-order system of equations of motion was integrated using the classical Runge–Kutta integration method. Figure 13 shows the response characteristics with initial conditions $\Delta\alpha = 5$ deg, $\Delta u = 0.1$ ft/s, $\Delta q = 0$ deg/s, and $\Delta\theta = 0$ deg. Disturbances in angle of attack and pitch rate decay quickly and come to zero within 1–2 s. The disturbances in velocity and pitch angle, on the other hand, persist for a while and decay slowly. In other words, disturbances in angle of attack and pitch rate decay rapidly during the short-period mode. During the phugoid mode, which continues after the decay of the short-period mode, the value of angle of attack remains nearly constant, and the pitch rate is close to zero.

Lateral-Directional Motion and Response

The analysis was made similar to that for the longitudinal motion. The equations given previously in the state-space form have the space variables $x = [\Delta\beta, \Delta p, \Delta r, \Delta\phi]^T$ and the state vector

Table 5 Lateral-directional dynamic characteristics

Variable	Dutch roll	Roll	Spiral
$T_{1/2}$, s	1.069	0.087	96.7
P, s	2.798	——	——
ζ	0.276	——	——
ω_n, rad/s	2.336	——	——

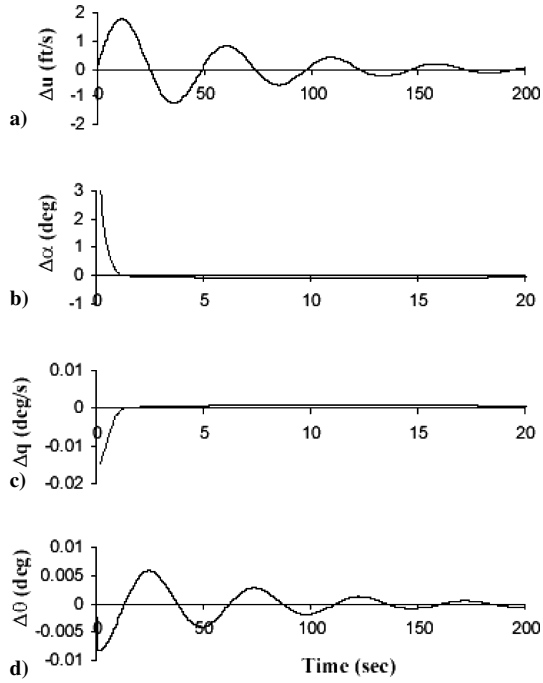

Fig. 13 Longitudinal response of the airplane with changes in a) velocity, b) angle of attack, c) pitch rate, and d) pitch angle.

$\eta = [\Delta\delta_a, \Delta\delta_r]$. The stability matrix A, as defined in Ref. 10, has the following values for the lateral-directional dynamics of the airplane:

$$A_{\text{lat}} = \begin{bmatrix} -0.256 & 0 & -0.964 & 0.116 \\ -7.964 & -7.905 & 1.126 & 0 \\ 5.088 & -0.186 & -1.055 & 0 \\ 0 & 1 & 0 & 0 \end{bmatrix}$$

Expanding this matrix yields another fourth-order characteristic equation of the form

$$A2\lambda^4 + B2\lambda^3 + C2\lambda^2 + D2\lambda + E2 = 0$$

The coefficients of the characteristic equation are $A2 = 279$, $B2 = 2568$, $C2 = 4388$, $D2 = 12{,}080$, and $E2 = 86$. The eigenvalues for this characteristic equation describe the modes of motion as

1) Dutch-roll mode, $\lambda_{\text{lat}1,2} = -0.646 \pm 2.246i$
2) Roll mode, $\lambda_{\text{lat}3} = -7.917$
3) Spiral mode, $\lambda_{\text{lat}4} = -0.00713$

A pair of complex roots, having damped oscillation with low frequency, represent the Dutch-roll motion. The Dutch-roll mode has a period of 2.798 s, and is well damped, requiring only 1.069 s to halve the amplitude. The root for the roll mode is real and negative, indicating a stable and heavily damped rolling motion. The predicted time to halve the amplitude is only 0.087 s. The root for the spiral mode is small and negative, indicating slowly convergent spiral motion. It takes 96.7 s to halve the amplitude. Table 5 presents the characteristic values for the lateral-directional motion.

Lateral-directional flying qualities of the airplane were examined from the published specifications.[9–11] Undamped natural frequency and damping ratio of the characteristic modes were calculated and are included in Table 5. The Dutch-roll mode has $\omega_n = 2.336$ rad/s and $\zeta = 0.276$ greater than the minimum required values for all

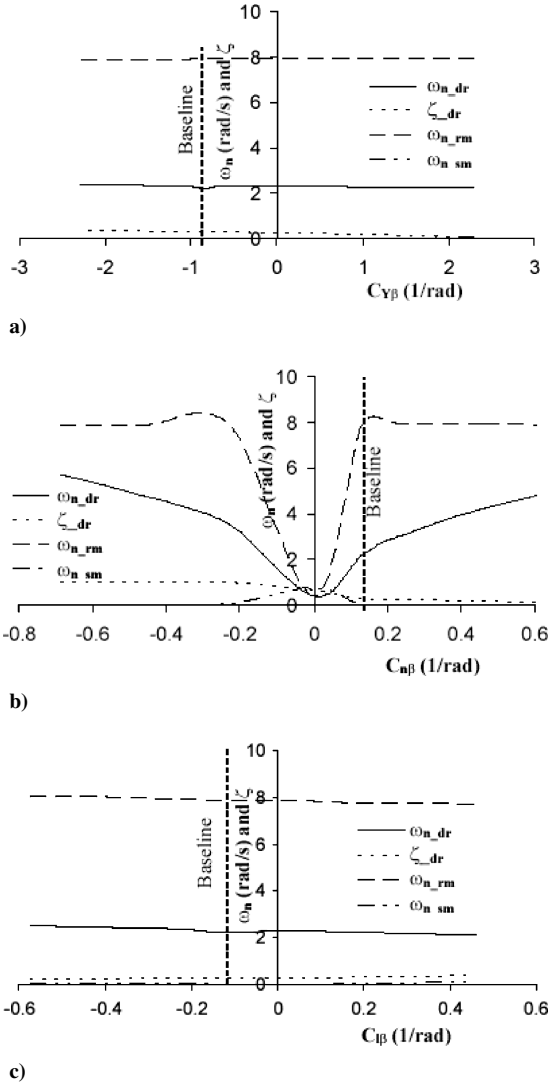

Fig. 14 Sensitivity analysis for ω_n and ζ parameters with changes in β derivatives: a) $C_{Y\beta}$, b) $C_{n\beta}$, and c) $C_{l\beta}$.

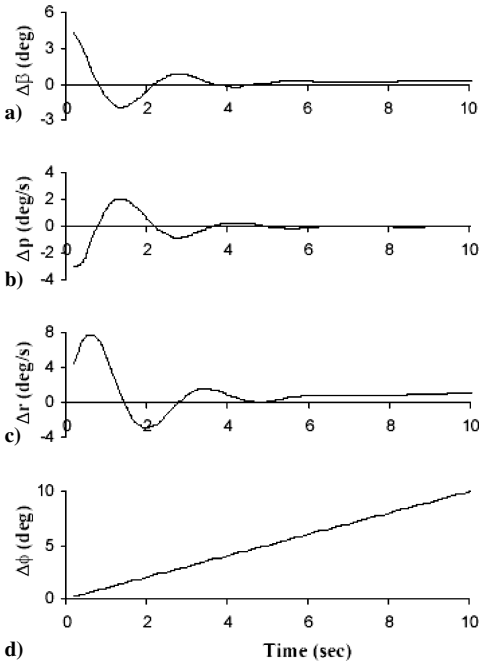

Fig. 15 Lateral–directional response of the airplane with changes in a) sideslip, b) roll rate, c) yaw rate, and d) bank angle.

flying quality levels and flight phases. Thus, the airplane is not expected to encounter any problem from the Dutch-roll mode. For the roll mode, the time constant was calculated from $\tau = -1/\lambda_{\text{lat3}}$ and found as $\tau = 0.126$ s. This value is well within the maximum roll-mode constant requirements for all of the flying quality levels and flight phases. The spiral mode already has a time-to-half-amplitude value of 96.7 s, and so is not included within the requirements.

The sensitivity of the lateral-directional ω_n and ζ values was determined for changes in the static stability derivatives, $C_{Y\beta}$, $C_{l\beta}$, and $C_{n\beta}$, as shown in Fig. 14. The side-force due to sideslip derivative, $C_{Y\beta}$, has an effect only on the Dutch-roll damping ratio. This is because the side force opposes the lateral velocity component, and thus it acts like a damping force. Yawing moment due to sideslip derivative, $C_{n\beta}$, has an effect on the size and location of the vertical tail. It is clear that $C_{n\beta}$ has a significant effect on Dutch-roll damping ratio, $\zeta_{\_dr}$, and undamped natural frequency, ω_{n_dr}, for values below the baseline, because they approach zero. Increasing the $C_{n\beta}$ has the effect of decreasing $\zeta_{\_dr}$ and increasing ω_{n_dr} and ω_{n_sm} values. The roll-mode frequency does not change. Increasing the rolling moment coefficient due to sideslip, $C_{l\beta}$, the so-called dihedral effect, increases the spiral stability and decreases Dutch-roll damping ratio and roll-time constant. The derivative $C_{l\beta}$ strongly depends on wing dihedral angle and sweep angle. In general, some balance between Dutch-roll damping and spiral stability can be attained by appropriate changes in the $C_{l\beta}$ value.

The airplane free response was also analyzed for lateral–directional motion. The corresponding fourth-order differential equations were integrated using the Runge–Kutta method. Figure 15 shows the time history of response characteristics for the initial conditions $\Delta\beta = 5$ deg, $\Delta p = 0$ deg/s, $\Delta r = 0$ deg/s, and $\Delta\phi = 0$ deg. The disturbance in the sideslip angle decays to zero within 5 to 6 seconds. The disturbance induces rolling and yawing motions. The rolling motion decays to zero along with the sideslip. However, the yawing motion does not go to zero. Instead, it assumes a nonzero steady-state value. This is due to the root becoming zero, which makes the motion involving yaw angle neutrally stable.

Suggested Geometric Changes

As a result of the wind-tunnel tests, geometric changes were made in airplane geometry to improve the flying qualities. These changes are included in three-view, shown in Fig. 1. The wing originally had a rectangular planform with constant NACA 4412 airfoil, adopted from another existing airplane. It was changed to a taper planform having a taper ratio of 0.4, with custom-designed root and tip airfoils for better performance. Wing area was reduced 13.5%, decreasing weight and parasite drag, and increasing the corresponding wing loading. This results in an improvement in airplane cruise efficiency, but requires a relatively high power input to meet the take-off field requirement. Wing fuselage juncture had some fairing to have better downstream flow. Horizontal tail area was increased 10% while tail arm length was reduced 15%. This change resulted in a 7.3% increase in horizontal tail volume coefficient. Vertical tail area was decreased 16.2%, causing 9.34% decrease in vertical tail volume coefficient. These changes in areas are expected to optimize the amount of lateral stability as compared with the amount of directional stability. The present test results yields a roll-to-yaw stability ratio, $C_l\beta/C_{n\beta} = -0.818$, indicating satisfactory stability for this type of cargo transport, as mentioned in Ref. 6. Also, the distance from the propeller disk plane to the center of gravity was reduced by as much as 16% by shortening the nose section. This alone would cause a direct reduction in the directional stability derivative $C_{n\beta}$ and the longitudinal stability derivative $C_{M\alpha}$, produced by the destabilizing effect of running propeller. Additionally, the fuselage cross section was more rounded to alleviate the degradation effect of downwash flow on the tail surfaces. The simple slotted flap used for the wing was not effective in lift production. Thus, the flaps had a new design having Fowler motion. All these suggested changes were incorporated with phase-two wind tunnel test model.

Conclusions

Stability and control characteristics of a 1/12 scale model of a high-wing cargo transport airplane were presented, as they were obtained from the Wichita State University wind tunnel at a Reynolds number of 0.92×10^6 and a Mach number of 0.2. The tests were made for power-off and stick-fixed conditions. Based on the results, the following conclusions can be drawn:

1) Drag due to extended landing gear is considered significant. It might be relatively low at some Reynolds number above the test value, but still the gear setting needs improvement to minimize interference and blockage effects.

2) Downwash effect at the conventional tail is considered high. Flow visualizations reveal that the flow from the wing–fuselage juncture swirls downstream and joins the flow on the upper side of the fuselage. This effect might be minimized by adding a dorsal fin, vortilon, or fairing parts, if changes on the fuselage shape are not sufficient.

3) The airplane has static stability about all three axes. The pitch stability derivative produces a neutral point at $0.57c$. Power effects would reduce the static margin of stability. There is a roll-to-yaw stability ratio of -0.818, considered satisfactory for this type of cargo transport.

4) Elevator, rudder, and aileron controls produce satisfactory control power. Flap requires a better design to improve takeoff and landing performance. Fowler-type slotted design is expected to provide relatively high lift performance.

5) For its cruise flight phase, the airplane flying qualities are better than level 3 for longitudinal motion and level 2 for lateral-directional motion. Changes are suggested in lifting surfaces so that there is a 7.3% increase in horizontal tail volume coefficient and a 9.34% decrease in vertical tail volume coefficient. These changes were incorporated into the airplane model used for phase-two wind tunnel tests.

Acknowledgments

The wind-tunnel tests reported in this paper were conducted while the author was with the Ayres Corporation of Georgia in the United States. The author acknowledges Fred P. Ayres, CEO and President of Ayres Corporation, for giving such a unique opportunity to work in design and testing of a new airplane. The author also thanks his family in Istanbul, Turkey for the support and encouragement he received during the completion of this research work.

References

[1]Federal Aviation Administration, Code of Federal Regulations 14, Parts 1 to 59, Part 23, revised Jan. 1, 2000.

[2]Biber, K., "Performance Predictions for a Single Propeller Driven Cargo Transport Airplane," AIAC-2005-056, *3rd Ankara International Aerospace Conference*, Ankara, Turkey, Aug. 22–25, 2005.

[3]Biber, K., "Prediction of Propeller Slipstream Drag Count for a Turboprop Airplane Performance," AIAA Paper 2005-0619, Jan. 2005.

[4]Biber, K., "Method of Determining Propeller Pitch Stops for a FAR 23 Airplane," [2000 SAE Transactions, SAE 2000-01-1692, Section 1], *Journal of Aerospace*, Sept. 2001, pp. 172–177.

[5]Biber, K., and Zumwalt, G. W., "Flow Field Measurements of a Two-Element Airfoil with Large Separation," *AIAA Journal*, Vol. 31, No. 3, 1993, pp. 459–464.

[6]Pope, A., and Harper, J. J., *Low-Speed Wind Tunnel Testing*, Wiley, New York, 1966.

[7]Perkins, C. D., and Hage, R. E., *Airplane Performance, Stability and Control*, Wiley, New York, 1949.

[8]Hoek, D. E., and Fink, R. D., *USAF Stability and Control DATCOM*, Vols. 1–4, Global Engineering Documents, Englewood, CO, Oct. 1960.

[9]Roskam, J., *Airplane Flight Dynamics and Automatic Flight Controls*, Part I, DAR Corporation, Lawrence, KS, 1995.

[10]Nelson, R. C., *Flight Stability and Automatic Control*, 2nd ed., McGraw–Hill, New York, 1998.

[11]Hodgkinson, J., *Aircraft Handling Qualities*, AIAA Education Series, AIAA, Reston, VA, 1999.

[12]Stinton, D., *The Design of the Aeroplane*, Oxford BSP Professional Books, London, 1983.

[13]*Flying Qualities of Piloted Aircraft*, MIL-HDBK-1797, U.S. Department of Defense, Washington, DC, Dec. 1997.

[14]*Military Specification Flying Qualities of Piloted Airplanes*, MIL-F-8785C, U.S. Department of Defense, Washington, DC, Aug. 1980.

[15]Cooper, G. E., and Harper, R. P. J., "The Use of Pilot Rating: The Evaluation of Aircraft Handling Qualities," NASA TN D-5153, April 1969.